

Optimization of the main-group and late-transition-metal elemental structures: Gallium, boron, zinc, cadmium, and manganese

Stephen Lee,* Roger Rousseau, and Cyndi Wells

Willard H. Dow Chemistry Laboratory, University of Michigan, Ann Arbor, Michigan 48109-1055

(Received 10 July 1992)

We demonstrate that a tight-binding Hamiltonian, to which a pairwise additive repulsive potential has been added, can qualitatively and semiquantitatively account for the elemental structures of gallium, boron, zinc, cadmium, and manganese. These structures represent the most complex structures found in the lighter elements of the Periodic Table ($N < 40$). We show that these structures result from the interplay of the number of valence electrons, the overlap of atomic orbitals, and geometrical features such as the number of triangles of bonded atoms and the angles between bonds. To illustrate this last point, we use the method of moments in a useful quantitative fashion. Finally, we account for the variation in cell parameters observed in binary noble-metal and main-group hexagonal closest-packed structures.

INTRODUCTION

Elemental structures have played a pivotal role in solid-state physics.¹ Not only do they give insight into the properties of the elements but they also pose challenging questions in their own right. The elements display highly disparate structures separated from one another by only minute differences in energy.² Slight miscalculations of binding energies therefore can lead to large shifts in atomic positions. Accurate optimizations of elemental crystal geometries have come to serve as a stringent test for electronic structure calculations.

One of the recent triumphs of modern electronic structure theory has been the accurate calculation of these small energy differences.^{3,4} For example, several researchers have studied the phase transitions induced by pressure on elemental silicon and germanium. These workers have not only been able to predict the order of these phase transitions (from diamond to white-tin, to simple hexagonal, and finally to the closest-packed structures) but also the actual pressure at which these transformations occur. It may fairly be said that accurate calculations of the differences in energy between competing structural alternatives are a current reality.

At the same time our understanding of the actual structural features responsible for these electronic energy differences has not progressed at a similar pace. For example it is well known that copper adopts the face-centered-cubic (fcc) structure while zinc adopts the hexagonal-closest-packed (hcp) structure. The experimental Hume-Rothery electron concentration rules show that this structural transformation is due to a change in the number of valence electrons.⁵ Although these rules predate modern quantum mechanics, no theory has yet been able to reproduce the entire range of the Hume-Rothery electron concentration rules nor specify the pertinent structural features. Similarly we can consider the elemental structure of gallium, which is a complex crystal with seven bonds per gallium atom.⁶ To date, one important study based on pseudopotentials has accounted for

the variation in bond lengths of this structure.⁷ However, earlier workers were unable to explain why the peculiar gallium structure itself is the ideal distortion mode for the various bonds.

In this paper we show that a method based on the tight-binding Hamiltonian can be used to account both qualitatively and semiquantitatively for elemental structures of main-group and later transition elements. This calculational approach uses valence-band variance scaling.^{8,9} This method in conjunction with the method of moments^{10,11} leads to a clear picture of the local structural effects responsible for the stability of a given crystalline phase. (Both variance scaling and the method of moments are described below.) We apply these rules to account for the rhombohedral packing of icosahedra in elemental boron, the corrugated layer structure of gallium, the somewhat two-dimensional character of zinc and cadmium, the variation in the cell parameters of hexagonally closest packed binary alloys, and the complex cubic packing of α -Mn.

CALCULATIONAL METHOD

Our theory is based on the tight-binding method, in which the repulsive portion of the interatomic energies is pairwise additive while the attractive portion is calculated from one-electron hopping integrals.¹² We therefore express the total energy, E_T as $E_T(r) = U(r) - V(r)$, where $U(r)$ is the hard-core interatomic repulsion energy, $V(r)$ is the attractive bonding energy, and r is a parameter which corresponds to the overall size of the system. We follow the idea of Heine, Robertson, and Payne¹³ that the repulsion energy is proportional to the coordination numbers of the atoms in the system, C . This repulsion energy is due to "Coulomb repulsion of the nuclei and the exclusion principle in the overlap of the atoms."¹³ As has been shown by Friedel and Cyrot-Lackmann,¹⁴

$$C = \gamma \int_{-\infty}^{\infty} E^2 \rho(E, r) dE ,$$

where $\rho(E, r)$ is the electronic density of states of the valence bands which itself is (among other things) a function of the overall size of the system, and γ is a proportionality constant. We therefore find that the total energy E_T is

$$E_T = \gamma' \int_{-\infty}^{\infty} E^2 \rho(E, r) dE + \int_{-\infty}^{E_F} E \rho(E, r) dE .$$

The first term on the right-hand side of the equation is the repulsive energy $U(r)$, while the second term is the attractive energy $-V(r)$. The term E_F refers to the Fermi energy for the system in question. We now follow the argument first discussed by Pettifor.¹⁵ We consider two systems which we label 1 and 2. The terms E_{T1} , U_1 , V_1 , E_{T2} , U_2 , and V_2 refer to the various energies of these two systems. We wish to calculate ΔE where $\Delta E = E_{T1} - E_{T2}$. It may be seen that

$$\Delta E = U_1(r_{1eq}) - V_1(r_{1eq}) - U_2(r_{2eq}) + V_2(r_{2eq}) ,$$

where r_{1eq} and r_{2eq} refer to the respective equilibrium sizes of the two systems.

We use the fact that we are interested in equilibrium geometries in the following way. Note that at equilibrium to first order in distance, $E_{Ti}(r)$ is constant. Therefore,

$$U_2(r_{2eq}) - V_2(r_{2eq}) \approx U_2(r_{2eq} + d) - V_2(r_{2eq} + d) .$$

In particular we choose a value for d such at $U_2(r_{2eq} + d) = U_1(r_{1eq})$. We now find that

$$\Delta E = \int_{-\infty}^{E_{F1}} E \rho_1(E, r_{1eq}) dE - \int_{-\infty}^{E_{F2}} E \rho_2(E, r_{2eq} + d) dE . \quad (1)$$

We determine the value r_{1eq} from the true experimental size factor and $r_{2eq} + d$ from the equality

$$\int_{-\infty}^{\infty} E^2 \rho_2(E, r_{2eq} + d) dE = \int_{-\infty}^{\infty} E^2 \rho_1(E, r_{1eq}) dE . \quad (2)$$

We note that the expression in Eq. (2) refers to μ_2 , the second moment of the valence bond electronic density of states, where $\mu_2 \equiv \int_{-\infty}^{\infty} E^2 \rho(E, r) dE$. In particular Eqs. (1) and (2) state that the difference in energy between two structural alternatives can be calculated from the knowledge of the one-electron density of states alone.

To calculate this one-electron density of states we use the tight-binding Hamiltonian

$$H_{t.b.} = \sum_{i,j} \beta_{ij} a_i^+ a_j + \sum_i \alpha_i a_i^+ a_i ,$$

where β_{ij} is a hopping integral between the i th and j th atomic orbitals (nonzero only if i not equal to j), α_i is the Coulomb energy of a given orbital, and a^+ and a are creation and annihilation operators. We furthermore follow the Mulliken-Wolfsberg-Helmholz approximation¹⁶ for off-diagonal β_{ij} , $\beta_{ij} = (K/2) S_{ij} (\alpha_i + \alpha_j)$, where K is a proportionality constant set at 1.75 and S_{ij} is the overlap integral between the i th and j th orbitals. The α_i values as well as the atomic orbital functions are chosen in conformity with Roothan-Hartree-Fock calculations on the individual atoms.¹⁷ Slight adjustments to these values

have been made in accordance with the work of the Hoffmann group on extended Hückel theory.¹⁸ In calculating the S_{ij} matrix elements we assume Slater-type orbitals (STO) with single or double zeta expansions.

In practice the above reduces to the following: When comparing two structural alternatives we calculate via standard k -space techniques the band structure of one compound at its true equilibrium size. For the second structure we scale its size so that its second moment exactly equals the second moment of the first. Then, using a rigid band model, we calculate the differences in energy of the two structures as a function of electron count. Finally we note that the constant γ' remains undetermined in this procedure. We therefore study only the structural shape and not the overall size of the geometries in question.

One of the chief strengths of this method comes from its connection with the method of moments.^{10,11} This moment method is based on the following observations: First, knowledge of μ_n , where $\mu_n = \int_{-\infty}^{\infty} E^n \rho(E, r) dE$ can be used to determine exactly the function $\rho(E, r)$. The most advantageous transform technique uses a continued fraction expansion¹⁹ (see Appendix). Second, the μ_n may be related to specific structural features, as μ_n is the sum of all closed paths of n steps in which one hops from one valence atomic orbital to the next. Third, the earliest μ_n , i.e., μ_0 , μ_1 , and μ_2 are all structure invariants: μ_0 is normalized to equal 1, μ_1 is just $Tr(H)$ and is therefore a constant sum of the Hartree-Fock atomic orbital energies, and finally μ_2 is treated as a constant in our variance scaling method [see Eq. (2)]. Finally we note that while it is necessary to know all the μ_n to determine $\rho(E, r)$ exactly, it is only the first few moments which control the principal features of the attractive energy $V(r)$.^{10,11} As we discuss below, knowledge of μ_3 through μ_6 is often sufficient in calculating energy differences between structures. This is particularly true if one uses the continued fraction expansion in conjunction with the upper and lower limits of $\rho(E, r)$ (which we call, respectively, E_u and E_l). This use of E_u and E_l can be important. The reason is that the higher moments are increasingly dominated by these two values. In the absence of exact knowledge of these higher moments, E_u and E_l have a significant role. (It should be noted that E_u and E_l are also related to local structural features; E_l depends on the coordination number C_i , and $E_u + E_l$ depends on the degree of nonalternancy.²⁰)

As an example of this method we consider band calculations for the fourth row of the main group. In particular we consider the elemental structures of Cu, Zn, Ga, Ge, As, and Se (elements 29–34 of the Periodic Table).²¹ Copper and zinc are, respectively, face-centered-cubic (fcc) and hexagonally-closest-packed (hcp), gallium adopts an unusual seven-coordinate structure discussed below, germanium forms in a diamond lattice, arsenic forms a three-coordinate two-dimensional puckered honeycombed sheet, while selenium adopts an infinite one-dimensional helix.²² We therefore need to compare $\rho(E, r)$ for each of these six structure types.

For meaningful comparisons we need to calculate the

electronic energies of each of these six structures for the same atom type. The Hartree-Fock energies of the valence $4s$ orbital ranges from $\alpha(4s) = -6.5$ to -22.9 eV, while the $4p$ orbital energies range from $\alpha(4p) = -5.7$ to -12.4 eV.¹⁷ The $\zeta(4s)$ exponent of the STO's range from $\zeta(4s) = 1.21$ for Cu to 2.4 for Se and similarly the $\zeta(4p)$ exponent ranges from $\zeta(4p) = 1.6$ to 2.1. With this great disparity in parameters, it would at first appear necessary to calculate 36 separate band structures, as for each of the six atom types we would need to compare all six of the possible structural alternatives. In practice it turns out not to be necessary. This is so as the differences in energy between structures are reasonably insensitive to changes in the Hartree-Fock parameters. In Fig. 1 we show the difference in energy between these six structures as a function of electron filling of the valence bands for a single set of atomic parameters. Values chosen were $\alpha(4s) = -16.0$ eV, $\alpha(4p) = -9.0$ eV, $\zeta(4s) = 2.16$, and $\zeta(4p) = 1.85$. These are the extended Hückel parameters for Ge developed by Thorn and Hoffmann.¹⁸ They correspond closely to the Hartree-

Fock values for this atom.²³ Germanium was chosen as it lies in the middle of the sequence of the six elements and therefore has average parameters with respect to the full series. The differences in energy plotted in Fig. 1(a) are between the structure of the labeled element and the diamond structure of germanium. Figure 1 is plotted with the convention that the curve with the most positive value at a given electron count corresponds to the most stable structure. For example, Ga is the most stable structure for a combined s and p band filling of 0.3–0.4. As we have previously discussed,^{9,11} the results in Fig. 1(a) match the elemental periodic trends exactly; each element is calculated as being most stable in its observed structure. What perhaps was not clear from our earlier work is that the method of moments can be used to quantitatively account for these results. In Fig. 1(b) we use only the values of μ_3 – μ_6 together with the various E_u and E_1 to calculate an approximate set of ΔE functions (see Appendix). It may be seen that Fig. 1(b) corresponds with the results of Fig. 1(a) in both the energy scale and the shape of the five functions. As our principal inputs are the values of μ_3 – μ_6 we can furthermore trace the provenance of a given structure's stability. In this respect it is useful to recall the effect of each individual moment.¹¹ These effects are summarized in Fig. 2. A large negative μ_3 stabilizes electron band fillings below 0.5, a large μ_4 stabilizes nearly filled band systems, and a large μ_6 stabilizes the half-filled band.²⁴ We recall that μ_n are the sums of all closed paths of n steps in which, via the hopping integral, one hops from one orbital to the next. Therefore, the μ_3 , μ_4 , and μ_6 values correspond in part to the number of atoms bonded in, respectively, triangular, square, and hexagonal arrangements. (As we will discuss later, other structural effects change the various moments. In particular the number of bonds and bond angles alter μ_4 .^{9,11}) We therefore conclude that the large number of triangles in the fcc and hcp structures stabilize these structures at low electron counts, the slightly fewer number of triangles stabilize the gallium system, the myriad of hexagons stabilize the diamond structure, and so forth.

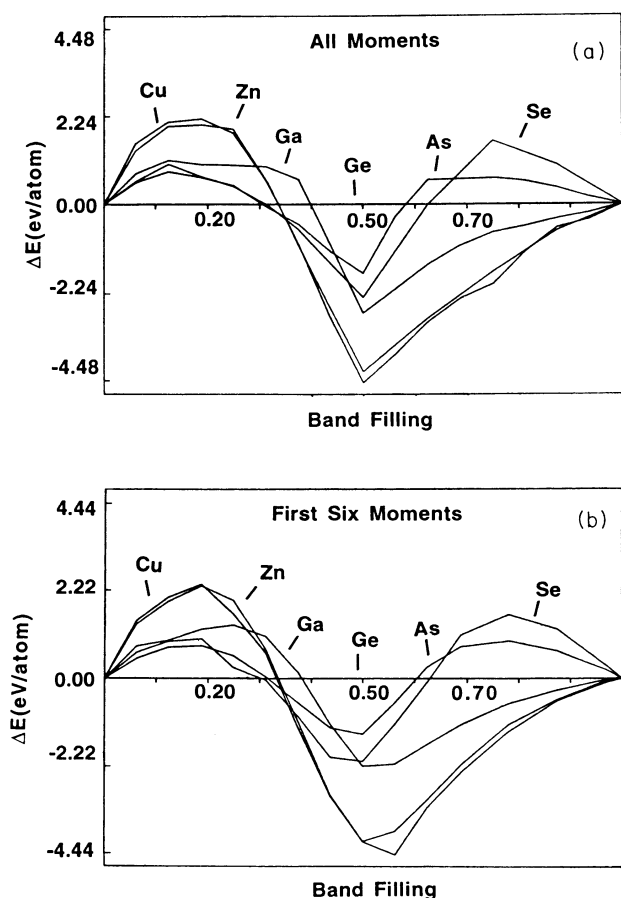


FIG. 1. Differences in energy between the structure types of elements 29–34 as a function of fractional s and p band filling. Energies are reported as the differences in energy to a fixed reference structure (in this case the diamond structure of Ge). In (a) we show the results for full band calculations while in (b) only the values of μ_3 – μ_6 , E_u , and E_1 were used. See discussion of Fig. 1 in the text for figure conventions.

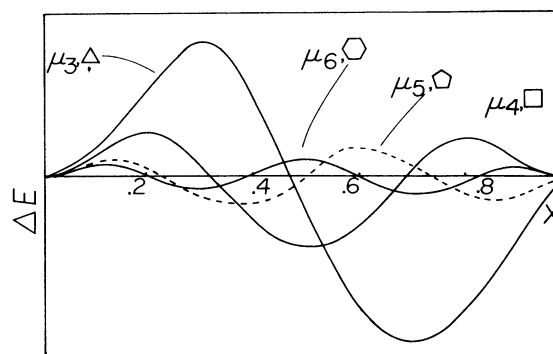


FIG. 2. Differences in energy between structures which have triangles, hexagons, pentagons, or squares in their structure as a function of x , the fractional band filling. Results are taken from Ref. 11. See discussion of Fig. 1 for figure conventions.

GALLIUM

The methods outlined above can be used to resolve the structure-energy relations of complex structures. As a first example we consider the stable form of gallium under standard conditions.⁶ The structure, illustrated in Fig. 3, is curious and unique. Each gallium atom is surrounded by seven other close-lying gallium atoms. One of these seven neighbors lies at a short distance of 2.47 Å away from the central gallium atom while the remaining six lie between 2.70 and 2.80 Å away. The overall coordination environment is remarkable in that these latter six atoms all lie in one hemisphere around the central gallium atom while the unusually close gallium neighbor lies in the center of the opposite hemisphere. The overall arrangement therefore resembles an umbrella which has been blown open by the wind.

This gallium structure is fundamentally different from those of its neighbors, which all have highly symmetrical first coordination environments. It is therefore useful to consider the relation of the gallium structure to its more symmetrical neighbors. The most convenient starting point is the two-dimensional closest-packed lattice, illustrated in Fig. 4(a). (It is instructive to note that rather isolated two-dimensional closest-packed layers are found in elemental zinc, and element adjacent to gallium in the Periodic Table.) The gallium structure can be derived from these sheets in two steps. First, one puckers the layers into the corrugated form shown in Fig. 4(b). The degree of puckering is controlled by the z parameter shown in this figure. These corrugated sheets are then stacked upon one another so that every gallium atom makes one bond with a gallium atom in either the sheet above or below it. A study of this geometry shows that there are three ways in which one can follow such a prescription (while keeping the c -axis parameter fixed). These three are illustrated in Fig. 5 along with their space-group labels. The true gallium arrangement has $Abma$ symmetry.

As a first problem, we compare the energies of these structural alternatives as a function of z , the parameter which controls the puckering of the sheets.²⁵ The value $z=0$ corresponds to unpuckered sheets. An increase in the value of z leads to more highly puckered sheets with ever shorter interlayer bonds. It may be seen in Fig. 6 that for all values of this parameter the experimentally observed $Abma$ structure is the lowest in energy. It may

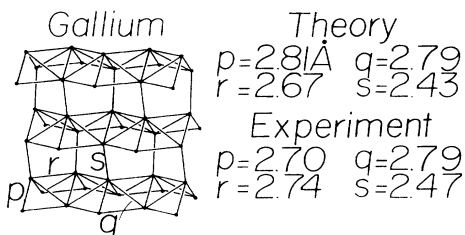


FIG. 3. Elemental structure of gallium. The four inequivalent bonds in this structure are labeled p , q , r , and s . Experimental and theoretically optimized values for these bond lengths are shown on the right side.

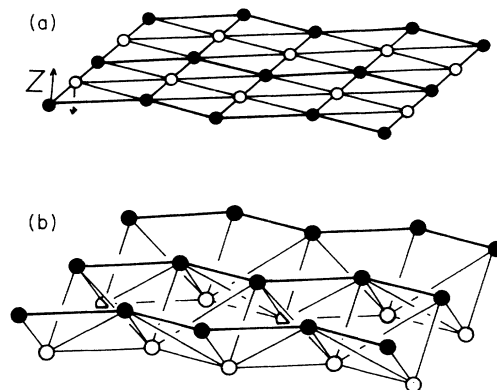


FIG. 4. Construction of the gallium structure from a 2D closest packing. (a) shows the undistorted 2D sheet while (b) shows the corrugated sheets found in the gallium structure.

also be seen that the optimal value of z is near the value $z=0.10$. The experimental value for this parameter is 0.095. In total there are four parameters which control the crystalline shape of the $Abma$ structure. These are the ratio of the cell axes, c/a and b/a , and the two atomic positional parameters x and z .²⁶ We therefore found the global energy minimum on this four-dimensional energy surface²⁷ using the variance scaling technique. Optimal values for the four parameters are shown in Table I. A comparison (assuming an optimal value for γ') of theoretical and experimental bond distances is shown in Fig. 3.

The above results demonstrate that a tight-binding theory with a pairwise additive repulsive energy contains the leading terms responsible for the gallium structure. We now can apply the method of moments to pinpoint the important structural features of the structure. We consider first the differences in energy between the $Abma$, $Icma$, and $Pnma$ structures. In Fig. 7 we plot these differences as a function of band filling (for $z=0.10$). In Fig. 7(a) we show these differences for a full set of band calculations while in Fig. 7(b) we use only the values of μ_3 , μ_4 , E_u , and E_l . It may be seen that these latter results contain the principal features of the full band calculations. In particular the shape of the curves resemble strongly the μ_3 curve shown in Fig. 2. We recall

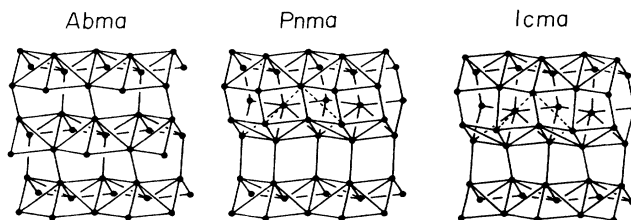


FIG. 5. The three alternate stackings of the corrugated sheets of Fig. 4 such that every atom makes one extra short bond with atoms either on the sheet on top or the sheet below. The 2.99-Å bond discussed in text is shown as a dotted line.

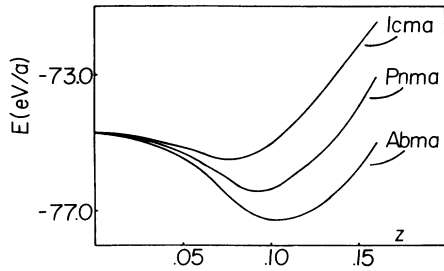


FIG. 6. Valence electronic energy per atom for the *Abma*, *Pnma*, and *Icma* structures as a function of z , the sheet puckering parameter.

that the actual values of μ_3 depend on the number of triangles of bonded atoms. The stability of the *Abma* structure therefore is due to the overabundance of triangles of bonded atoms in *Icma* and *Pnma* structures. As the three polymorphs are identical within the puckered two-dimensional sheets, this overabundance must occur in intersheet interactions. An examination of the crystal geometries shows the existence of an interlayer 2.99-Å bond in the *Icma* and *Pnma* structures not present in the

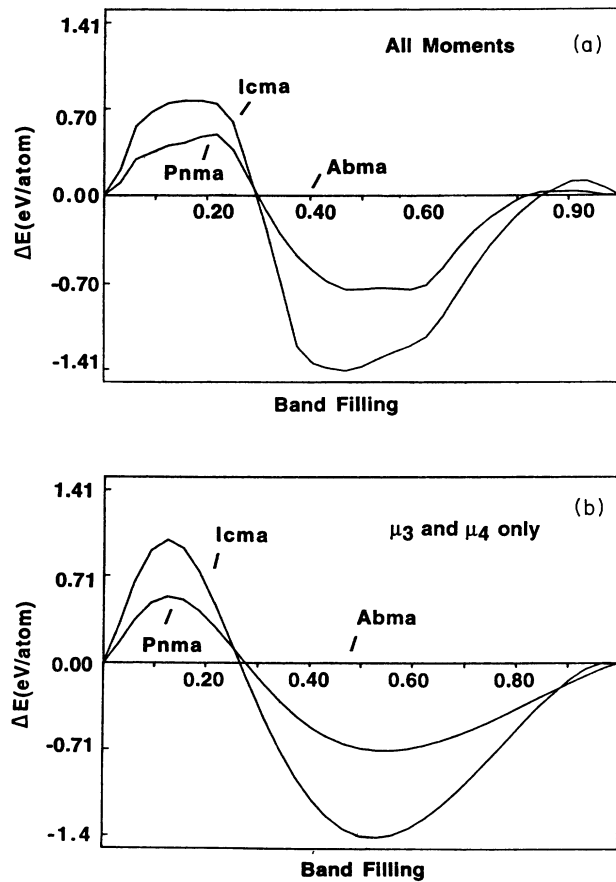


FIG. 7. Difference in energy between the *Icma*, *Pnma*, and *Abma* structures as a function of fractional band filling. In (a) we show the full band calculation while in (b) we use the continued fraction approximation using only μ_3 , μ_4 , E_u and E_1 . See discussion of Fig. 1 for figure conventions.

TABLE I. Crystal parameters for the gallium structure.

Parameter	Experiment ^a	Theory
a	4.516 Å	
c/a	1.690	1.61
b/a	0.994	0.94
Ga x	0.044	0.035
Ga z	0.095	0.100

^aAt 4.2 K.

Abma structure. This bond is indicated by the dotted lines in Fig. 5. Calculations both with and without the H_{ij} elements of this bond reveal that it is indeed this bond which is principally responsible for the shape of the curves in Fig. 8. Furthermore, it may be seen that the presence of this bond leads to intersheet triangular interactions. We conclude the stability of the *Abma* structure is due to the elimination of these unwanted triangles.

We now turn to the factors which control the optimal parameters of the *Abma* structure. We restrict ourselves here to the parameter with the strongest energy dependence, z . In Fig. 8(a) we show the results of a full band

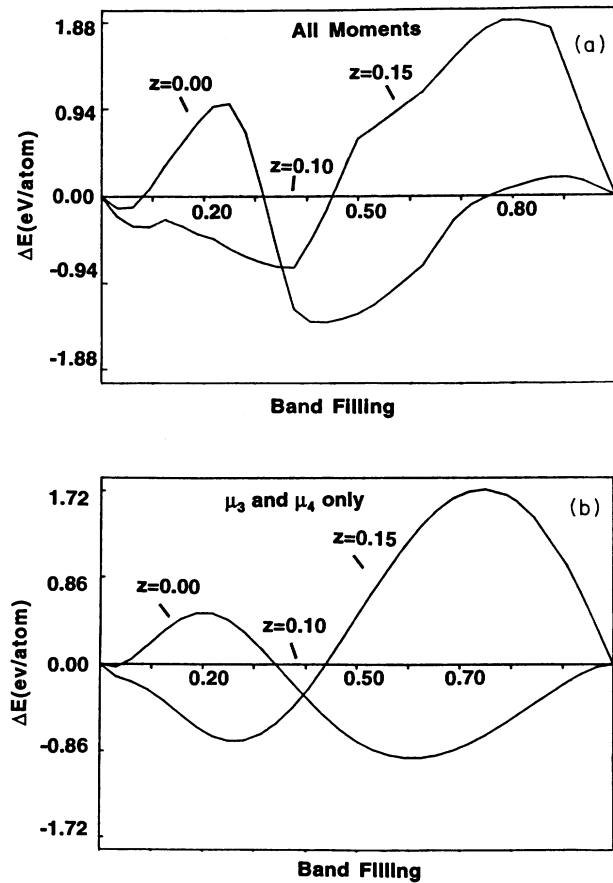


FIG. 8. Differences in energy between the *Abma* structure when the z parameter equals 0.00 and 0.15 and when it equals 0.10 as a function of fractional band filling. In (a) we show the full band calculation and in (b) the continued fraction approximation using only μ_3 , μ_4 , E_u , and E_1 . See discussion of Fig. 1 for figure conventions.

calculation for $z=0.00, 0.10,$ and 0.15 . In Fig. 8(b) we use only $\mu_3, \mu_4, E_u,$ and E_1 . It may be seen that the principal features of the curves in Fig. 8(a) are reproduced by Fig. 8(b). These results can be understood in the following manner: At $z=0$ one has unpuckered two-dimensional (2D) closest-packed sheets with little interlayer interaction. As each atom lies on six different triangles in 2D closest packing, there is a surfeit of triangles for an s - and p -band filling of 0.375 (the band filling of gallium). In changing z from $z=0.0$ to $z=0.1$ one replaces the *intralayer* triangular interactions with an *interlayer* hexagonal interaction (these hexagons can be seen in Fig. 5). However, by the time the point $z=0.15$ is reached, the interlayer hexagons have almost completely supplanted the aforementioned triangles. At this point, we have too few triangles to be compatible with the fractional band filling of 0.375. The optimal value for $z=0.10$ is therefore due to an optimization of the number of triangles.

ZINC AND CADMIUM

Zinc and cadmium form in the hcp structure.²² The hcp structure type has only one size-independent parameter, the ratio of the c and a crystallographic cell axes (c/a). For a c/a value of 1.63 the hcp structure is a true

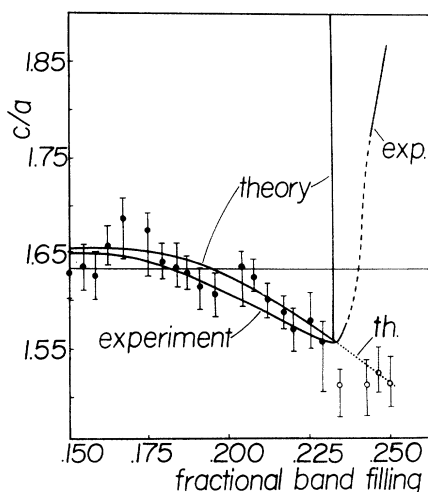


FIG. 9. The c/a ratio in noble metal and main group metal hcp structures as a function of fractional s and p band filling. The experimental curves are the average of the following binary alloy systems: Au-Hg, Au-Cd, Au-In, Au-Sn, Au-Zn, Ag-Ga, Ag-Hg, Ag-As, Ag-Sb, Ag-In, Ag-Cd, Ag-Sn, Ag-Al, Az-Zn, Cu-Ga, Cu-Ge, and Cu-Zn. The theoretical curves are the optimized values using variance scaling, a rigid band model, and zinc atomic parameters. Small circles indicate the actual results of our optimizations. Filled circles indicate global minima, empty circles indicate local minima. The bars around each circle indicate values within 0.005 eV per unit cell of the associated minimum. The fork in the theory curve near a fractional band filling of 0.235 indicates the presence of a double minimum. The dashed line indicates a region without experimental data. The ideal c/a ratio of 1.63 is indicated as a horizontal line. A 90 k -point mesh was used for all hcp optimizations.

closest packing and every atom has exactly twelve nearest neighbors.

It is well established that the ratio of the c/a axes in noble-metal and main-group metal alloys depends strongly on the number of valence electrons.²⁸ This dependence is shown in Fig. 9. It may be seen that at fractional band fillings near a value of 0.15 the experimental c/a ratio is near the ideal value of 1.63. For the slightly greater electron filling of 0.23, the c/a ratio is lowered to 1.55. There is then a discontinuous jump in this c/a ratio as one approaches a fractional band filling of 0.25. Finally the hcp structure does not exist for noble-metal—main-group metal alloys at higher electron concentrations than 0.25 except in the case of relativistic heavy atoms. These experimental results may be compared with our theoretical results which are also shown in Fig. 9.²⁹ It may be seen that the qualitative trends of the experimental curves are reproduced in our calculations. For electron concentrations near an s and p band filling of 0.15, the ideal c/a ratio of 1.63 is observed. Near a band filling of 0.23 the c/a ratio reduces to a value near 1.55. Finally at a fractional band filling of 0.235 there is a discontinuous jump in the c/a ratio. While in the true zinc experimental structure this ratio rises to 1.86 (in cadmium the c/a ratio is 1.89), in our theory a pure two-dimensional sheet is the preferred structure. Thus while we are able to explain why the sheets become separated in elemental zinc or cadmium, we have not properly modeled the restoring force which prohibits further increase in the c/a ratio beyond the c/a ratio of 1.86.

The qualitative agreement between the experimental and theoretical curves allows us to determine the principal structural feature responsible for the increase in the c/a ratio in elemental zinc (and cadmium). We find that at band fillings greater than 0.21 the three-dimensional closest packings have a surfeit of triangles of bonded atoms. Both raising and lowering the c/a ratio from 1.63 reduces the size of μ_3 . As one increases the band filling the only effective way to reduce μ_3 , however, is to increase the c/a ratio. The two dimensional packing is therefore adopted for the same reason that the $Abma$ structure is observed for elemental gallium. As we discussed in the preceding section, by the point the band filling is 0.375 the two-dimensional closest-packed ($z=0.0$ geometry) structure in turn gives way to the gallium structure with even fewer triangles.

BORON

With the exception of sulfur, no element displays greater polymorphism in its crystal structures than boron.²² Nine polymorphs have been reported with unit cells ranging from a twelve-atom rhombohedral cell to a 1708-atom cubic cell. The structures of five of these polymorphs have been fully resolved. In all five, regular icosohedra play a significant role. Structures derived from icosohedra play an equally ubiquitous role in molecular boron chemistry.³⁰ We show this icosohedron from two perspectives in Fig. 10.

The nature of the bonding within boron icosohedra is well understood.³¹ Wade's rules for clusters associate 26

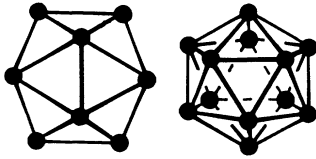


FIG. 10. Two views of the icosohedron. On the left it is seen down a twofold axis while on the right it is viewed down a threefold axis.

valence electrons with bonds internal to the icosohedra (intraicosohedral bonds). These rules have been amply tested both experimentally and theoretically. There is therefore no current need to reinvestigate these intraicosohedral bonds. The same cannot be said for intericosohedral bonds. While it is known that three center (triangular) and two center bonds are important, the exact relation between these bonds and electronic energy is not well established.

In our calculations we will concentrate on the simplest of the boron polymorphs, the *R*-12 structure, which contains twelve atoms in a rhombohedral cell. Each unit cell of this structure contains one icosohedron whose center can be placed at the cell axes origin. As boron has three valence electrons, there are a total of 36 valence electrons per primitive unit cell; of these 36 electrons, 26 are used in intraicosohedral bonds and 10 in intericosohedral bonds.

There are five crystallographic parameters which control the shape of the *R*-12 polymorph. They are the rhombohedral cell angle α and the atomic x and z fractional coordinates for the two symmetry-inequivalent boron atoms. In Table II we show our optimal values for these parameters using our variance scaling technique.³² The six inequivalent bonds in the *R*-12 structure are found experimentally to have the lengths of 2.021, 1.787, 1.785, 1.777, 1.733, and 1.709 Å. Theoretically (if we assume an optimal value of γ') we find these bond lengths to be respectively 1.90, 1.88, 1.89, 1.79, 1.56, and 1.73 Å. While our calculated bond lengths are roughly in the correct order in going from longest to shortest lengths, the numerical agreement is poor. The average error in bond lengths is 0.09 Å.

As in the preceding studies on gallium and zinc, it is instructive to compare the *R*-12 structure with reasonable crystallographic equivalents in order to elucidate the most significant structural features of the *R*-12 structure. As our primary interest is with the intericosohedral bonds we consider alternative packings of these icosohedra. In particular, for the sake of numerical simplicity we consider systems which have exactly one icosohedron per unit cell. Furthermore we assume that the icosohedra line up in such a way as to preserve some portion of the point-group symmetry of the individual clusters. Of the three types of rotational axes (fivefold, threefold, and twofold) only the threefold and twofold axes are compatible with translational crystalline symmetry. These symmetry axes are found in the trigonal, orthorhombic, and

TABLE II. Crystal parameters for the boron *R*-12 structure.

Parameter	Experiment	Theory
a	5.057 Å	
α	58.06°	56.7
$B(1)x$	0.010	0.00
$B(1)z$	0.657	0.67
$B(2)x$	0.221	0.22
$B(2)z$	0.632	0.62

monoclinic crystal classes. We consider here only the higher symmetry trigonal and orthorhombic lattices. We recall that there are four types of orthorhombic Bravais lattices (primitive, face centered, end centered, and body centered) and only two types of trigonal Bravais lattices (primitive and rhombohedral). We therefore need to explore these six different Bravais lattices. We therefore optimized elemental boron assuming that its structure corresponded to one of these six different lattice types. In each case we maintained a perfect icosohedral shape for the individual clusters. In Fig. 11 we compare the differences in energy of these polymorphs. It may be seen that at an s and p band filling of 0.375 (which corresponds to the fractional band filling of elemental boron) the experimentally observed rhombohedral form (*R*-12) is the most stable. At lower electron counts the primitive trigonal and face-centered orthorhombic structures are more stable while at higher band fillings the *C*-centered and primitive orthorhombic cells are energetically preferred.

We now apply the method of moments to determine the specific structural causes for these energy differences. In particular, we will consider the primitive trigonal form as an example of a polymorph stable at low band fillings and the *C*-centered orthorhombic lattice as an example of a phase stable at high band fillings. It is instructive to first consider in detail the pertinent structural features of these phases. In Fig. 12 we illustrate the rhombohedral (*R*-12), *C*-centered orthorhombic, and primitive trigonal

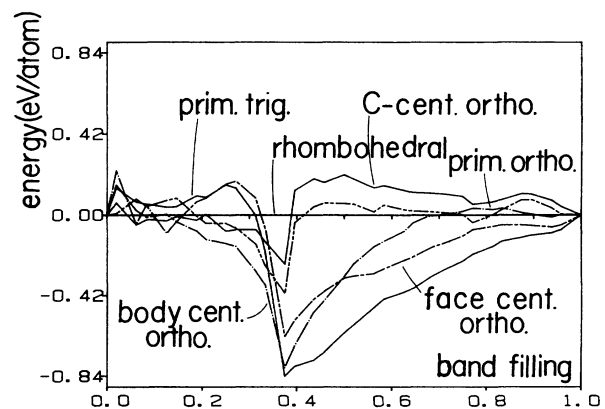


FIG. 11. Differences in energy between the high-symmetry Bravais lattices where there is one icosohedra per unit cell as a function of fractional band filling. At the fractional band filling of boron, 0.375, the experimentally observed rhombohedral form is preferred. See the discussion of Fig. 1 for figure conventions.

polymorphs. In the middle of Fig. 12 we portray the rhombohedral structure viewed down primarily the hexagonal [001] axis. It may be seen that in the (hexagonal) **a-b** crystallographic plane the intericosohedral bonds form both triangles and squares of bonded atoms. There are two such triangles and three such squares per unit cell. Also shown in Fig. 12 is a triangle of atoms connected to the regular icosohedra by 1.71 Å bonds. This triangle represents the base of an icosohedron in the next-higher plane in this structure. These 1.71 Å bonds lie on intericosohedral hexagons of bonded atoms. We note that these 1.71 Å bonds point radially outward from the icosohedron. On the bottom of Fig. 12 we illustrate the primitive trigonal cell viewed down primarily the [001] axis. It is identical to the rhombohedral cell within the **a-b** plane. It differs in the positioning of the out-of-plane icosohedra which in the primitive trigonal structure lie directly above the lower icosohedra. The bases of four of the out-of-plane icosohedra are shown in Fig. 12. It may be seen that the interlayer cavities are octahedra. As octahedral faces are triangles, these out-of-plane octahedra increase the μ_3 value for the primitive trigonal lattice significantly.

On the top of Fig. 12 we illustrate the *C*-centered or-

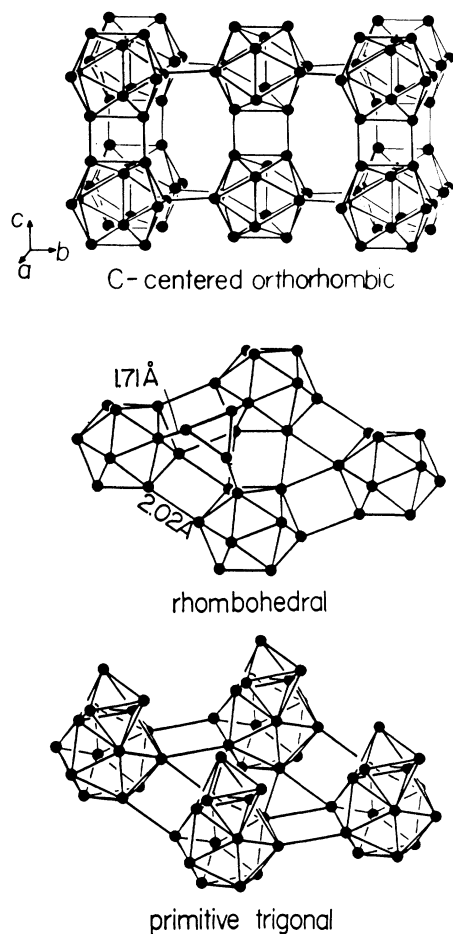


FIG. 12. The optimal structures of the *C*-centered orthorhombic, rhombohedral, and primitive trigonal Bravais lattices of single icosohedra.

thorhombic structure viewed primarily down the [100] direction. It may be seen that there are squares involving intericosohedral bonds in this structure normal to both the **a** and **b** directions. Bond angles between these intericosohedral and the intraicosohedral links therefore are as small as 90°. Harder to see are the hexagons of bonds normal to the **c** axis. It is interesting to note that the **a-b** plane of the icosohedra found in the *C*-centered orthorhombic structure is identical to sheets found in the rhombohedral structure.

In Fig. 13 we show the differences in energy between these three structures using only μ_3 , μ_4 , E_u , and E_l . These curves reproduce many of the qualitative features of the full band calculations. In particular, it may be seen that the primitive trigonal structure is stable for low fractional band fillings while the *C*-centered orthorhombic structure is stable for high band fillings. These differences in energy can be explained in terms of local structural features. The difference in energy between the primitive trigonal and the rhombohedral geometry is due to the larger μ_3 in the former geometry. This difference in μ_3 is due to the formation of octahedral cavities between the individual icosohedral units (octahedra have eight triangular faces).

The difference in energy between the rhombohedral and *C*-centered orthorhombic structures is due to the different *fourth* moments for the two structures. The *C*-centered orthorhombic structure has twice as many squares of bonded atoms as does the rhombohedral structure. Although this contributes to the larger μ_4 of the *C*-centered cell, the principal difference in μ_4 is caused by the intericosohedral bond angles. In particular, μ_4 is minimized when the intericosohedral bonds point radially outward. The six 1.71 Å bonds in the rhombohedral structure are oriented in exactly this manner. By contrast none of the intericosohedral bonds in the *C*-centered cell are aligned in such a fashion. We therefore conclude that the rhombohedral Bravais lattice is energetically preferred for two reasons. On the one hand it minimizes the number of intericosohedral triangular interactions, while on the other it minimizes the μ_4 term by maintaining the proper intericosohedral bond angles.

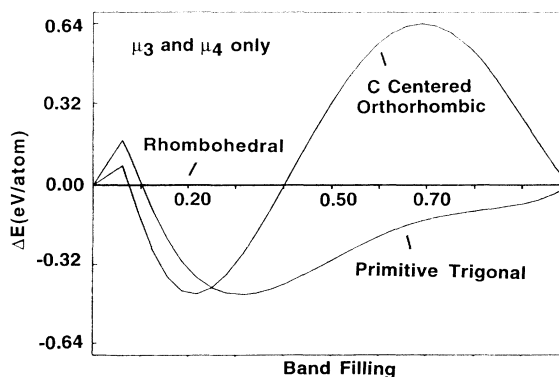


FIG. 13. Difference in energy between the primitive trigonal, *C*-centered orthorhombic, and the rhombohedral Bravais lattices of single icosohedra as a function of fractional band filling. The results shown here are the continued fraction results using only μ_3 , μ_4 , and E_1 .

MAGANESE

Manganese has the most complex of all elemental structures.²² The thermodynamically stable form ($< 727^\circ\text{C}$) α -Mn has 58 atoms in a body-centered cubic unit cell. A portion of this cell is illustrated in Fig. 14. The crystal structure of α -Mn has been determined six times,²² and from this data it would appear that the structure belongs to the body-centered cubic space group $I\bar{4}3m$ with four symmetry-inequivalent sites. There are, however, still unresolved structural issues in the α -Mn structure.³³ α -Mn is known to be antiferromagnetic. On the basis of symmetry conditions alone, one may deduce that two of the symmetry-inequivalent sites are each divided into two sets of magnetically inequivalent sites. Hence the $I\bar{4}3m$ space group is not compatible with the magnetic structure. A space group which is compatible with the lower symmetry is the body-centered tetragonal cell of $I4_2m$.

Earlier studies have applied tight-binding techniques to rationalize the structures of the transition elements.³⁴ We have shown in our earlier work that the α -Mn structure is the most stable structure at an electron count of seven s , p , and d electrons per atom when compared to the other known transition-metal structures and also when using first-row transition element parameters. This comparison was made with the β -Mn, body-centered-cubic, fcc, hcp, and σ -phase structures. This earlier study correctly accounted for the structures of the group 5–group 12 elements of the Periodic Table in much the same way as our results shown in Fig. 1 correctly account for the structures of elements 29–34. These results suggest that the electrons involved in the antiferromagnetism of α -Mn do not control the principal character of this structure.

We have, therefore, optimized this structure using the variance scaling method. Due to the large size of this

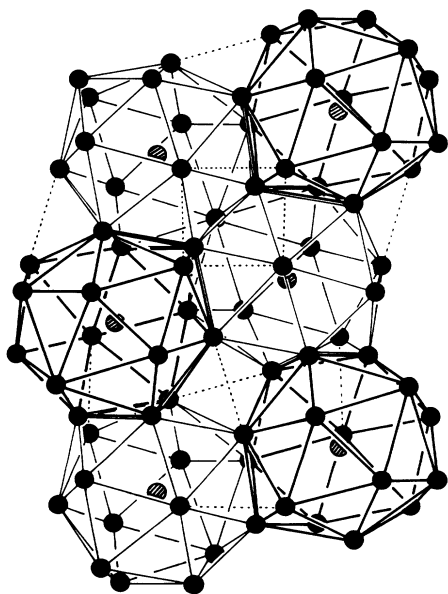


FIG. 14. The structure of α -Mn.

TABLE III. Crystal parameters for the α -Mn structure.

Parameter	Experiment	Theory
a	8.913 Å	
Mn(II) x	0.318	0.29
Mn(III) x	0.357	0.34
Mn(III) z	0.035	0.02
Mn(IV) x	0.090	0.06
Mn(IV) z	0.282	0.28

calculation we have only explored the energy surface near the experimental parameter values. Assuming the symmetry is $I\bar{4}3m$ there are five atomic positional parameters. In Table III we show our calculated optimized values for these parameters. Errors are slightly larger than in the main-group element optimizations, the average error being 0.017. We can also use our method to probe the space-group assignment of the x-ray crystallographic group. We therefore allowed the Mn atoms to lower themselves from cubic symmetry to the $I4_2m$ tetragonal space group. We find that the $I4_2m$ solution is considerably lower in energy than the optimal cubic $I\bar{4}3m$ geometry (by at least 4 eV per unit cell). At this time, we have not made an exhaustive search among all subgroups of $I\bar{4}3m$ and it is therefore possible that there are subgroups with even lower energy. Nevertheless our data suggest it would be worthwhile to see if indeed, as the magnetic data suggests, α -Mn is subtly distorted from the accepted cubic space group.

CONCLUSION

In this article we have used a tight-binding theory to study the structures of the lighter elements in the periodic table. We have examined first the trends in structure found in a single period. We have then studied the curious structures of α -Mn, gallium, boron, zinc, and cadmium. In all cases we have found that our tight-binding method can account qualitatively and semiquantitatively for the experimentally observed crystal types. The only structure-dependent integrals calculated in our method are the two-center overlap integrals between valence atomic orbitals. Exchange, Coulombic, self-consistent-field, and correlated electron motion effects have been ignored except insofar as they contribute either to the pairwise repulsion energy (which itself is also estimated from the two-center overlap integrals) or to the structurally invariant Hartree-Fock atomic parameters. Together with previously published results for clusters, alloys, and intermetallic systems,^{8,9} our findings present a startlingly simple picture of the interactions principally responsible for the shape (but not size) of metallic and covalent solids and molecules.

The type of structure adopted by an element is principally governed by the overlap of the element's valence atomic orbitals. The effect of these valence atomic orbitals can be readily decomposed in a finite cluster-type expansion (moment expansion). The principal feature which controls the stability of an elemental structure is the local coordination environment around the atoms.

The most important relation is between the number of triangles of bonded atoms and the fractional band filling. For example, both the elemental zinc and elemental gallium structures are the result of optimizing the number of triangles of bonded atoms with respect to fractional band fillings of 0.25 and 0.375. In a similar fashion there exists an interplay between the number of squares and bond angles and the fractional band occupancy, as we illustrated in the case of elemental boron. These relationships are pithily described by continued fraction functions.

These effects hold equally true for metals such as gallium as for nonmetals such as boron. Within the context of our method the oftentimes-made distinction between the directional covalent nonmetallic bonds and the non-directional metallic bonds obscures more than it illuminates. We find instead that the structures of metals and nonmetals are due to the overlap of the same valence atomic orbitals. The critical difference between metals and nonmetals arises from the fact that in the regime of small band fillings, structures rich in triangles are energetically stable. Band calculations on such structures show that such triangle-based structures rarely have band gaps. We conclude that in those cases where the structure type is controlled by electron count (versus size) the nondirectionality of metallic bonds is principally a consequence of the high coordination numbers associated with triangle-rich structures.

ACKNOWLEDGMENTS

We would like to thank Ami Hatta for helping with the calculations on the gallium structure and Professor Meigan Aronson for suggesting the calculations on α -Mn in a tetragonal space group. This research was supported by funds from the Petroleum Research Fund administered by the American Chemical Society. Our research would not have been possible without the computer programs developed by R. Hoffmann, M.-H. Whangbo, M. Evain, T. Hughbanks, S. Wijeyesekera, M. Kertesz, C. N. Wilker, C. Zheng, J. K. Burdett and, G. Miller.

APPENDIX

We state here the formulas needed to generate $\rho(E)$ from the values of μ_n . It is useful to define the variable Δ_n ,

$$\Delta_n = \begin{vmatrix} \mu_0 & \mu_1 & \cdots & \mu_n \\ \mu_1 & \mu_2 & \cdots & \mu_{n+1} \\ \vdots & \vdots & & \vdots \\ \mu_n & \mu_{n+1} & \cdots & \mu_{2n} \end{vmatrix}.$$

We may then define the sequences a_i and b_i , where

$$\Delta_n = a_0 a_1 \cdots a_n \Delta_{n-1},$$

$$\int E^{p+1} B_p(E) \rho(E) dE = -a_0 \cdots a_p (b_0 + b_1 + \cdots + b_p),$$

$$B_p(E) = (b_{p-1} + E) B_{p-1}(E) - a_{p-1} B_{p-2}(E),$$

where

$$B_{-1}(E) = 0 \text{ and } B_0(E) = \mu_0.$$

We now use E_u and E_l to find a and b , where $E_u = -b + 2\sqrt{a}$ and $E_l = -b - 2\sqrt{a}$. The formula for $\rho(E)$ is then

$$\rho(E) = \text{Im} \left\{ \frac{a_0}{E + b_0 - \frac{a_1}{E + b_1 - \frac{a_2}{E + b_2 - f}}} \right\}, \quad (\text{A1})$$

$$f = \frac{E + b + \sqrt{(E + b)^2 - 4a}}{2}.$$

In Eq. (A1) the number of a_i and b_i corresponds to the number of moments in use. For example Eq. (A1) is the correct function to use when one knows only $\mu_0 - \mu_4$. For the case of $\mu_0 - \mu_6$ an extra row would be added to the fraction on the right side of Eq. (A1). These formulas only hold in the case of purely continuous functions.

*Author to whom correspondence should be addressed.

¹E. P. Wigner and F. Seitz, in *Solid State Physics*, edited by F. Seitz and D. Turnbull (Academic, New York, 1955), Vol. 1, p. 97.

²C. A. Coulson, *Valence* (Oxford Press, New York, 1952).

³These results are based on density-functional theory. See P. Hohenberg and W. Kohn, *Phys. Rev.* **136**, B864 (1964); W. Kohn and L. J. Sham, *ibid.* **140**, A1133 (1965). A review of the density-functional method is given by C. J. Callaway and N. H. March, in *Solid State Physics*, edited by H. Ehrenreich, F. Seitz, and D. Turnbull (Academic, New York, 1984), Vol. 38.

⁴Y. K. Vohra, K. E. Brister, S. Desgreniers, A. L. Ruoff, K. J. Chang, and M. L. Cohen, *Phys. Rev. Lett.* **56**, 1944 (1986); M. T. Yin and M. L. Cohen, *ibid.* **45**, 1004 (1980), *Phys. Rev. B* **24**, 6121 (1981); **26**, 5668 (1982); S. Fahy and S. G. Louie, *ibid.* **36**, 3373 (1987); H. Olijnyk, S. K. Sikka, and W. B. Holzapfel, *Phys. Lett.* **103A**, 134 (1984); J. Z. Hu and I. L. Spain, *Solid State Commun.* **51**, 263 (1984).

⁵W. Hume-Rothery and G. V. Raynor, *The Structure of Metals*

and Alloys (Institute of Metals, London, 1962); W. Hume-Rothery, in *Phase Stability in Metals and Alloys*, edited by P. S. Rudman, J. Stringer, and R. I. Jaffee (McGraw-Hill, New York, 1976), p. 3.

⁶F. Laves, *Z. Kristallogr. Kristallgeom. Krystallophys. Kristallchem.* **84**, 256 (1933); C. S. Barrett, *Adv. X-Ray Anal.* **5**, 33 (1961).

⁷V. Heine and D. Weaire, *Solid State Physics* (Academic, New York, 1970).

⁸This method was proposed independently for AB (main group-transition metal) by D. G. Pettifor and R. Podlucsky, *Phys. Rev. Lett.* **53**, 1080 (1984) and for the Peierls distortion by J. K. Burdett and S. Lee, *J. Am. Chem. Soc.* **107**, 3063 (1985). Other papers whose results are based on this method include D. G. Pettifor, *J. Phys. C* **19**, 285 (1986); J. C. Cresconi and D. G. Pettifor, *J. Phys. Condens. Matter.* **3**, 495 (1991), and the references cited below in Ref. 9.

⁹S. Lee, *J. Am. Chem. Soc.* **113**, 101 (1991); **113**, 8611 (1991); L. M. Hoistad, S. Lee, and J. Pasternak, *ibid.* **114**, 4790 (1992); L. M. Hoistad and S. Lee, *ibid.* **113**, 8216 (1991); S. Lee, *Acc.*

- Chem. Res. **24**, 249 (1991); S. Lee, *Inorg. Chem.* **31**, 3063 (1992); S. Lee, L. M. Hoistad, and S. T. Carter, *New J. Chem.* (to be published).
- ¹⁰F. Cyrot-Lackmann, *Surf. Sci.* **15**, 535 (1968); F. Ducastelle and F. Cyrot-Lackmann, *J. Phys. Chem. Solids* **31**, 1295 (1970); **32**, 285 (1971); J. P. Gaspard and F. Cyrot-Lackmann, *J. Phys. C* **6**, 3077 (1973).
- ¹¹J. K. Burdett and S. Lee, *J. Am. Chem. Soc.* **107**, 3050 (1985); **107**, 3063 (1985).
- ¹²The addition of a pairwise repulsive energy is crucial to the tight-binding model. See D. J. Chadi, *Phys. Rev. B* **19** 2074 (1979); **29** 785 (1984). A review of the various tight-binding methods is given in A. P. Sutton, M. W. Finnis, D. G. Pettifor, and Y. Ohta, *J. Phys. C* **21**, 35 (1988). The use of a pairwise additive repulsion term can be derived from density-functional theory. See W. M. C. Foulkes and R. Haydock, *Phys. Rev. B* **39**, 12 520 (1989). See also W. A. Harrison, *ibid.* **34**, 2787 (1986).
- ¹³V. Heine, I. J. Robertson, and M. C. Payne, in *Bonding and Structure of Solids*, edited by R. Haydock, J. E. Inglesfield, and J. B. Pendry (Royal Society, London, 1991).
- ¹⁴J. Friedel, *Adv. Phys.* **3**, 446 (1954); F. Cyrot-Lackmann, *J. Phys. C* **C1** 67 (1970).
- ¹⁵D. G. Pettifor, *J. Phys. C* **19**, 285 (1986).
- ¹⁶M. Wolfsberg and L. Helmholz, *J. Chem. Phys.* **20**, 83 (1957).
- ¹⁷E. Clementi and C. Roetti, *At. Data Nucl. Data Tables* **14**, 177 (1974); J. B. Mann, *Atomic Structures Calculations, 1: Hartree-Fock Energy Results for Elements Hydrogen to Lawrencium* (Clearinghouse for Tech. Lit., Springfield, 1967).
- ¹⁸Many important atomic parameters are used and discussed in R. Hoffmann, *J. Chem. Phys.* **39**, 1397 (1963); A. B. Anderson and R. Hoffmann, *ibid.* **60**, 4271 (1974); A. R. Rossi and R. Hoffmann, *Inorg. Chem.* **14**, 365 (1975); P. J. Hay, J. C. Thibeault and R. Hoffmann, *J. Am. Chem. Soc.* **97**, 4884 (1975); M. Elian and R. Hoffmann, *Inorg. Chem.* **14**, 1058 (1975); R. H. Summerville and R. Hoffmann, *J. Am. Chem. Soc.* **98**, 7240 (1976); J. W. Lauher and R. Hoffmann, *ibid.* **98**, 1729 (1976); S. Komiyama, T. A. Albright, and R. Hoffmann, *Inorg. Chem.* **17**, 126 (1978); T. Hughbanks, R. Hoffmann, M.-H. Whangbo, K. Stewart, O. Eisenstein, and E. Canadell, *J. Am. Chem. Soc.* **104**, 3876 (1982); D. Thorn and R. Hoffmann, *Inorg. Chem.* **17**, 126 (1978).
- ¹⁹A review of the various methods for calculating the density of states from the sequence of moments is given in S. Glanville, A. T. Paxton, and M. W. Finnis, *J. Phys. F* **18**, 693 (1988).
- ²⁰C. A. Coulson and G. S. Rushbrooke, *Proc. Cambridge Philos. Soc.* **36**, 193 (1940).
- ²¹An earlier report of this work, without the decomposition into moments is given in S. Lee, *J. Am. Chem. Soc.* **113**, 8611 (1991). A similar report is given in J. C. Cressoni and D. G. Pettifor, *J. Phys. Condens. Matter* **3**, 495 (1991).
- ²²J. Donohue, *The Structures of the Elements* (Wiley, New York, 1974).
- ²³These Ge extended Hückel parameters can be compared to J. B. Mann's values (Ref. 17) of $\alpha(4s) = -15.15$ eV and $\alpha(4p) = -7.33$ eV and E. Clementi and C. Roetti's values of $\zeta(4s) = 2.01$ and $\zeta(4p) = 1.70$.
- ²⁴The location of the nodes in the difference of energy curves are sensitive to the values of E_u and E_l . A tail in the DOS running to the left or right shifts the nodes in the direction of the tail. See discussion of this in S. Lee, *J. Am. Chem. Soc.* **110**, 8000 (1988).
- ²⁵We use the same parameters for the 4s and 4p orbitals as in the calculations of the preceding section on the series of elements from Cu-Se.
- ²⁶The nonstandard setting used is given in Ref. 10 of L. M. Hoistad, S. Lee, and J. Pasternak, *J. Am. Chem. Soc.* **114**, 4790 (1992). This earlier paper gives a preliminary report of the results presented here.
- ²⁷We find minima on the energy surface by a method a steepest descent. In order to ensure that we have found a global minimum we choose several different starting values for the parameters. In general, except in the case of more complex molecules, we have not had problems with false local minima.
- ²⁸T. B. Massalski, in *Physical Metallurgy*, edited by R. W. Cahn and P. Haasen (North-Holland, Amsterdam, 1983), p. 186.
- ²⁹We used the established extended Hückel parameters for zinc. These are $\alpha(4s) = -12.41$ eV, $\alpha(4p) = -6.53$ eV, $\zeta(4s) = 2.01$, and $\zeta(4p) = 1.70$. As before, the reported results are quite insensitive to the above values and no attempt has been made here to optimize the parameters to improve agreement with experiment. These Zn values are taken from J. Silvestre and T. A. Albright, *Isr. J. Chem.* **23**, 139 (1983).
- ³⁰For a recent review, see *Electron Deficient Boron and Carbon Clusters*, edited by G. A. Olah, K. Wade, and R. E. Williams (Wiley, New York, 1991).
- ³¹K. Wade, *Adv. Inorg. Chem. Radiochem.* **18**, 1 (1976); R. W. Rudolph and W. R. Pretzer, *Inorg. Chem.* **11**, 1974 (1972); R. E. Williams, *ibid.* **11**, 210, 1971; D. M. P. Mingos, *Acc. Chem. Res.* **17**, 311 (1984); W. N. Lipscomb, *Boron Hydrides* (Benjamin, New York, 1963); E. L. Muetterties and W. H. Knoth, *Polyhedral Boranes* (Wiley, New York, 1968).
- ³²We used the well-established extended Hückel parameters for boron. These are $\alpha(2s) = -15.2$ eV, $\alpha(2p) = -8.5$ eV, $\zeta(2s) = 1.3$, and $\zeta(2p) = 1.3$. These values are taken from A. B. Anderson and R. Hoffmann, *J. Phys. Chem.* **60**, 4271 (1974). They may be compared to the atomic Hartree Fock parameters of Ref. 17. J. B. Mann (Ref. 17) gives $\alpha(2s) = -13.46$ eV and $\alpha(2p) = -8.43$ eV. Clementi and Roetti (Ref. 17) give values of $\zeta(2s) = 1.288$ and $\zeta(2p) = 1.211$.
- ³³See discussion in T. Yamada, N. Kunitomi, Y. Nakai, D. E. Cox, and G. Shirane, *J. Phys. Soc. Jpn.* **28**, 615 (1970); T. Yamada, *ibid.* **28**, 596 (1970).
- ³⁴A seminal study on transition-metal structures is given in D. G. Pettifor in *Metallurgical Chemistry*, edited by O. Kubaschewski (Her Majesty's Stationary Office, London, 1972), p. 191. This earlier study, however, does not include p orbitals and therefore fails to produce the correct structure type on the right side of the transition series. In L. M. Hoistad and S. Lee, *J. Am. Chem. Soc.* **113**, 8216 (1991) it is shown that the inclusion of the p function allows one to account for the structures of the σ -phase, χ -phase, and the various noble-metal structures. In this earlier work first-row transition-metal parameters the extended Hückel iron parameters are used. There are $\alpha(4s) = -9.10$ eV, $\alpha(4p) = -5.32$ eV, $\alpha(3d) = -12.6$ eV, $\zeta(4s) = 1.9$, and $\zeta(4p) = 1.9$. For the 3d functions a double-zeta expansion was used: $\zeta_1(3d) = 5.35$, $\zeta_2(3d) = 2.00$, $C_1(3d) = 0.5505$, and $C_2(3d) = 0.6260$. These values taken from R. H. Summerville and R. Hoffmann, *J. Am. Chem. Soc.* **98**, 7240 (1976). We use these parameters again here in our current work on α -Mn.